Journal of Materials Chemistry C

Accepted Manuscript

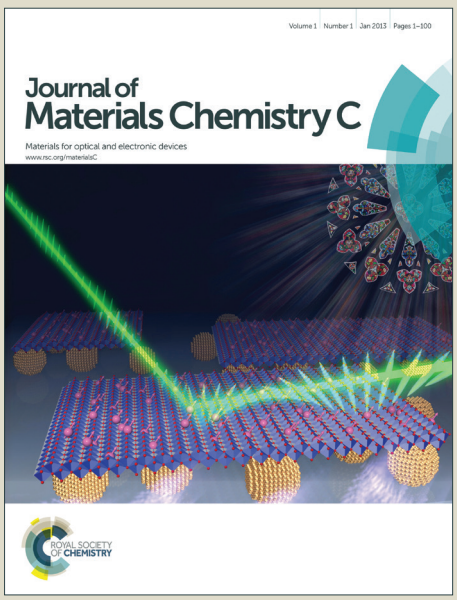

ROYAL SOCIETY OF CHEMISTRY

www.rsc.org/materialsC

Sulfur-doped graphene laminates for EMI shielding applications

Faisal Shahzad[a,b], Pradip Kumar[a] ,Seunggun Yu[a] , Seunghwan Lee[a], Yoon-Hyun Kim[c], Soon Man Hong[a,b], Chong Min Koo[a,b,*]

[a]*Center for Materials Architecturing, Korea Institute of Science and Technology, Hwarangno 14-gil 5, Seongbuk-gu, Seoul 136-791, Republic of Korea*

[b]*Nanomaterials Science and Engineering, University of Science and Technology, 176 Gajung-dong, 217 Gajungro, Yuseong-gu, Daejeon 305-350, Republic of Korea*

[c]*R & D Center, Chang Sung Corporation,11B-9L, Namdong Industrial Area 320, Seunggicheon-ro, Namdong-gu, Incheon, Republic of Korea*

*Corresponding author. Tel.: +8229586872; Fax: +8229585309.

E-mail address: koo@kist.re.kr (C.M. Koo).

Abstract

Herein, for the first time, we demonstrate that a laminated structure of sulfur-doped reduced graphene oxide (SrGO) provides significant potential for electromagnetic interference shielding application. In this work, SrGO was prepared through the reaction between graphene oxide and hydrogen disulfide (H_2S) gas at elevated temperatures. The doping degree of S was controlled through varying the time and temperature of the reaction and achieved the maximum doping content of 5.6 wt %. Because of the n-type doping contribution of S atom to the doped graphene, SrGO laminate did not only reveal 47% larger electrical conductivity (75 S cm^{-1}) than undoped reduced graphene oxide laminate (51 S cm^{-1}) but also revealed 119% larger EMI shielding effectiveness (33.2 dB) than undoped one (15.5 dB) at the same sample thickness.

Keywords: Graphene, Sulfur doping, Laminate, Conductivity, Electromagnetic interference shielding

1 Introduction

Electromagnetic interference (EMI) shielding materials have been gaining a rapidly growing attention as the fast surge in utilization of electronic devices, such as cellular phones, televisions, radios, loudspeakers, and laptops. It has greatly increased the potential applications for EMI in our daily life.[1-4] The deteriorating effect of EMI noise is not limited to the malfunctioning of electronic devices but it also threatens human health.[5, 6]

Among many EMI shielding materials, in recent years, graphene-based materials have been extensively investigated as EMI shielding. The efficiency of materials for EMI shielding largely depends on electrical conductivity. Graphene, possessing excellent electrical conductivity is a suitable candidate for EMI shielding applications.[7, 8] Liang et al. developed processable solution of functionalized graphene in epoxy matrix and obtained an EMI shielding value of 21 dB for 15 wt % filler loading.[9] Song et al. developed polymer free graphene mixed Fe_3O_4 hybrid system where EMI shielding of 20 dB was achieved at a thickness of 0.3 mm.[10] Chen et al. developed chemical vapor deposited graphene on nickel foam that its subsequent composite with poly(dimethylsiloxane) resulted in a high EMI shielding performance of 22–25 dB at a thickness of 1 mm.[11] Verma et al. used a high-energy ball milling technique to synthesize barium ferrite decorated reduced graphene oxide nanocomposite that provided a large EMI shielding value of 32 dB at a thickness of 3 mm.[12] Despite the extensive studies on its use as EMI shielding material, the full potential of graphene has not been explored yet for this application because the mass-production process of reduced graphene oxides, including harsh chemical oxidation process, disturbs the sp^2 electronic structure of graphene, resulting in reduction of the electrical conductivity of graphene. Recently, the n-type doping of graphene with heteroatoms, such as

nitrogen, was considered as an effective way to recover electronic property of the graphene.[13, 14] Sulfur is a relatively new n-type dopant and its potential has not yet been fully explored for applications other than in electrochemistry.[15-17] Zhou et al.[18] and Denis et al.[19] reported that S doped graphene forms a thiophene-like structure that imparts positive influence on the electronic and magnetic properties of graphene, nevertheless utilization of S doped graphene for EMI shielding application is not explored and no report on the effect of S doping on EMI shielding properties is available in open literature.

In this work, for the first time, we demonstrate that S-doped graphene in a laminated structure reveals much larger EMI shielding effectiveness than undoped laminate at very small thicknesses. This observation is attributed to the n-doping effect of S-doped graphene, which improves the electrical conductivity.

2 Experimental

2.1 Materials

Natural graphite was purchased from Bay Carbon (SP-1, USA). Other chemicals, including hydrochloric acid (37%), sulfuric acid (95%–97%), hydrogen peroxide (30%), and potassium permanganate (99%) were purchased from Sigma Aldrich. Hydrogen sulfide (H_2S) gas was diluted with nitrogen gas in a ratio of 5/95 (v/v). Custom-made quartz tubes were used for thermal reduction and doping reactions. All chemicals were used as received without additional purification.

2.2 Synthesis of sulfur-doped reduced graphene oxide laminates

First, graphene oxide (GO) was prepared through the modified Hummers method.[20, 21] Sulfur-doped reduced graphene oxides (SrGO) were synthesized through the thermal annealing of GO for 1 h at three different temperatures of 250, 650, and 1000 °C. One hour annealing time

was split in two different steps: First, thermal annealing step for S doping on graphene under H_2S gas atmosphere for 10 or 30 min followed by the second step of post annealing under argon atmosphere for 50 or 30 min. The prepared GO powders were loaded in a tubular quartz tube reactor surrounded by furnace (ESI Fig. S1). It was heated to the reaction temperature and the powder was reacted with mixed flow of H_2S gas for predetermined reaction time and then cooled down to room temperature to collect the resulting S-doped graphene samples. For the representative sample name of 1000SrGO-30, the number before SrGO represents the reaction temperature (in °C) whereas the latter number represents the reaction time (in minutes) under H_2S gas atmosphere. The detail procedure and schematic of the doping reaction is illustrated as scheme1. SrGO laminates were prepared through pelletization using an automated press under 15 t load for 10 min having diameter of 10mm and thickness of 0.14 mm which were then cut in toroid shape for measuring EMI shielding properties.

2.3 Synthesis of reduced graphene oxide laminates

Reduced graphene oxide (rGO) was synthesized using a similar protocol as SrGO, except that the one hour thermal annealing was performed under argon atmosphere without H_2S gas treatment.

2.4 Materials characterization

The morphologies of products were characterized using transmission electron microscopy (TEM, JEM 2100F, JEOL, Japan) and field-emission scanning electron microscopy (FE-SEM, Inspect F50, FEI, USA) techniques equipped with an energy dispersive X-ray spectrometer (EDX). Samples for TEM measurement were prepared by drying a drop of dilute graphene/ethanol suspension on a TEM grid. Samples for SEM of powder samples were performed by compressing small amount of powder on carbon tape, whereas the samples for

characterizing the cross sectional view of laminates was obtained by cutting the laminate in liquid nitrogen. X-ray photoelectron spectroscopy technique (XPS, K-Alpha, Thermo Scientific, USA) with Al Kα as the X-ray source and a power of 72 W was used to investigate the chemical structures and compositions. Raman spectroscopy was conducted using Raman Spectrometer LabRam HR Ar-ion laser 514 nm (Jobin-Yvon, France). The DC electrical conductivity of the samples was determined using four-pin probe (MCP-TP06P PSP) method with Loresta GP meter (MCP-T610 model, Mitsubishi Chemical, Japan). The samples for determining electrical conductivity were made with a diameter of 10 mm and thickness of 140 μm. EMI shielding effectiveness of each sample was measured using ENA5071 Agilent Network Analyzer with a coaxial wire method consisting of toroidal-shaped specimen (ϕ_{out} = 7 mm, ϕ_{in} = 3.04 mm, and thickness of 140 ± 5 μm). The incident electromagnetic waves had a power of 0 dBm, which corresponds to 1 mW.

3 Results and Discussion

3.1 Microstructural analysis of SrGO

Fig. 1a,b shows typical TEM and SEM micrographs of 1000SrGO-30 sample with wrinkled and folded features. SrGO sheets randomly overlap, retaining the layered structure of graphene as a result of high temperature thermal reduction and evolution of oxygen containing functional groups. Fig. 1c exhibits photographs of pristine GO and 1000SrGO-30 samples. The SrGO sample reveals a porous fluffy morphology due to considerable volume expansion of GO with significant weight loss and a strong exothermic reaction during the sulfur doping reaction at elevated temperatures. (See ESI Fig. S2 for TGA and DSC thermograms). The presence and distribution of sulfur on the graphene sheets was confirmed through EDX analysis and elemental

mapping, as shown in Fig. 1d,e, respectively. Elemental mapping confirmed the sulfur presence over entire scanned area, suggesting that doping occurred throughout the available substitutional sites. Fig. 1f reveals the fractured surface of 1000SrGO-30 laminate sample with graphene sheets compacted in longitudinal direction, while inset shows the samples for electrical conductivity and EMI shielding measurement.

3.2 XPS observations

Fig. 2a shows the C1s spectra of GO deconvoluted in three Gaussian-type peaks with binding energies of 284.5 eV (non-oxygenated C ring, C=C and C–C), 286.5 eV (hydroxyl and epoxy, C–O), and 288.2 eV (carboxyl, O–C=O).[22] Fig. 2b reveals the C1s spectra of 1000SrGO-30 deconvoluted in five Gaussian-type peaks with binding energies of 284.5 eV (non-oxygenated C ring, C=C and C–C), 285.6 eV (epoxy, C–O, C–S), 287.2 eV (carboxyl, O–C=O), 289.1 eV (C=O) and a π–π* shake-up signal at 291.1 eV that is typical for sp^2-hybridized carbon).[23, 24] The intensity of oxygenated groups in GO considerably decreases and the C=C/C–C bond becomes dominant in thermally reduced sulfur-doped graphene sample.

Fig. 2c shows S2p spectra of 250SrGO-30. Two types of C–S bonding spectra were observed associated with –C–SO_x–C– (x = 2, 3, 4) at 168.5 and 169.7 eV and –C–S–C– bridges arising from $2p_{3/2}$ and $2p_{1/2}$ of thiophene–S due to spin–orbit coupling at 163.73eV and 164.9eV.[25, 26] The result suggests that sulfoxide bridges are stable at lower temperatures where H_2S gas reacts with oxygen functional groups of graphene, however at higher temperatures of 650 and 1000 °C (Fig. 2d–e), we detect a single –C–S–C– bonding configuration as the sulfoxide bridges disappeared during heating because of thermal instability at high temperatures.[16] In contrast, the rGO samples prepared at 250, 650 and 1000 °C did not show any S signal and correspondingly no S2p spectra of rGO could be recorded from XPS analysis.

Fig. 3a–c shows the full scan XPS spectra of all the graphene samples. Sulfur signal from S2p peak was observed in doped samples. Table 1 summarizes the elemental compositions of all the doped and undoped graphene samples. The 250SrGO-10 sample shows sulfur signal that slightly increased with increasing doping time. No sulfur was detected in the 250rGO sample. The samples of 650SrGO-10 and 650SrGO-30 exhibited similar patterns of increasing sulfur content with doping time (from 0.83 to 1.89 atom %). For 1000SrGO-10 and 1000SrGO-30 samples, sulfur content increased from 2.02 to 2.19 atom % with no sulfur in the 1000rGO sample. The largest achievable sulfur content was 2.19 atom % in 1000SrGO-30 sample, which corresponds to 5.6 wt %. We observed increase in sulfur content with increasing of doping time and temperature, however, we noted that the sulfur doping is almost saturated at 1000^{o} C. Further high temperatures or doping time may not be sufficient for increasing the sulfur content as we assume the sulfur doping more depends on the available substitutional and defect sites. During course of heating from lower temperatures to high temperature, more vacancies are generated due to loss of oxygenated species and opportunity for sulfur atom to get bonded with carbon host increased. Increase in doping time provide access for diffusion of H_2S gas to more sites through graphene powder and sulfur content increased. Once the available sites for (-C-S-C) bond are occupied, further heating or doping time will not result in increase of doped sulfur content which means the appropriate doping condition to get maximum sulfur content may be at 1000 ^{o}C with small doping time. The sulfur contents in our samples are among one of the largest values reported so far via utilizing various precursors to obtain –C–S–C– type of bonding configuration.[15, 25, 27]

Table 1 Elemental composition from XPS observations

Sample	XPS (atom %)			C/O
	C	S	O	–
250rGO	86.20	–	13.80	6.24
250SrGO-10	85.38	0.25	14.37	5.94
250SrGO-30	86.75	0.28	12.96	6.69
650rGO	89.29	–	10.71	8.33
650SrGO-10	86.41	0.83	12.76	6.77
650SrGO-30	85.90	1.89	12.21	7.03
1000rGO	93.72	–	6.28	14.92
1000SrGO-10	93.85	2.02	4.13	22.72
1000SrGO-30	94.74	2.19	3.07	30.85

3.3 Raman spectra

Fig. 4a–c shows the Raman spectra of GO, rGO and SrGO samples. All samples exhibit characteristics of graphitic D and G band peaks around 1350 and 1583 cm^{-1}. The G band, originating from in-plane vibration of sp^2 carbon atoms, is the most prominent feature of the majority of graphitic materials, whereas, D band is characteristic of defects and disorders in the graphene lattice.[25, 26] A larger I_D/I_G ratio ascribes to more defects and distortions. We observed increase in Id/Ig ratio with further decrease of temperature and doping time, indicating that sulfur causes some structural distortion in graphene due to different atomic size.[28, 29] The G band, which is sensitive to chemical doping, has been reported to show red shift for n-type substitutional doping or when electron-donating groups are added to the system.[15, 26] Interestingly, we observed a change in the G band spectra of SrGO, whereby a clearly visible red

shift from 1594 cm^{-1} to lower wave numbers was witnessed after S doping. The red-shift (10~11 cm^{-1}) was more prominent in 1000SrGOs sample (Fig. 4a), whereas shift of 6~8 cm^{-1} was observed for 650SrGOs (Fig. 4b) and 2~3 cm^{-1} for 250SrGOs (Fig. 4c). The Raman spectroscopy results together with XPS and EDX elemental mapping observations strongly confirmed the sulfur bonding with carbon in (–C–S–C–) state with n-type doping. Similar n-type doping has previously been observed in sulfur and nitrogen doped graphenes.[14, 15, 26, 30]

3.4 Electrical conductivity

Electrical conductivities of doped and undoped graphene laminates were also examined (Fig. 5). A large increase in conductivity values was observed for samples doped at high temperature (1000 °C). This observation can be ascribed to n-type doping contribution from S atoms. The 1000SrGO-30 laminate sample revealed 47% larger electrical conductivity value (75 S cm^{-1}) than undoped reduced graphene oxide laminate sample (51 S cm^{-1}) processed at the same annealing temperature. Theoretically, the phenomenon can be understood from the equation $\sigma = en\mu$, where σ is conductivity, μ is mobility, and n and e are concentration and charge of electrons, respectively. S atoms possess more valence electrons than C; therefore, when substitutionally present in the graphene lattice, they provide extra electrons to the graphene layers that increase the charge concentration and density of electrons. The extra electrons become free carriers and shift the Fermi level up from the Dirac point of pristine graphene towards the conduction band, contributing to the overall conductivity increase of S doped graphene.[27, 29, 31]

3.5 EMI shielding

EMI shielding effectiveness (SE), the materials' ability to shield an electronic device from electromagnetic radiation, is given by the following equation:[8]

$$SE_T\,(dB) = 10\log\,(\frac{P_I}{P_T}) \quad (1)$$

where (P_I) is the incident and (P_T) is the transmitted or remaining power in decibels (dB). EMI shielding is the sum of contributions from reflection, absorption and multiple internal reflections of radiations from a material body. SE_R (called as shielding due to reflection) is related to the impedance mismatch between air and shielding material, whereas SE_A (called as shielding due to absorption) is the energy dissipation of the electromagnetic microwaves in the shield. Total EMI shielding effectiveness (SE_T) can be expressed as,

$$SE_T = SE_R + SE_A \quad (2)$$

In a two port vector network analyzer, SE_T can be determined through calculation of the reflectance (R), transmittance (T), and absorbance (A) coefficients, which can be correlated to scattering parameters (S_{11}, S_{12}, S_{21}, S_{22}) as:

$$R = |S_{11}|^2 = |S_{22}|^2\,,\ T = |S_{12}|^2 = |S_{21}|^2$$

SE_R and SE_A can be written in terms of scattering parameters as:

$$SE_R = 10\log\left(\frac{1}{1-R}\right) = 10\log\left(\frac{1}{1-|S_{11}|^2}\right) \quad (3)$$

$$SE_A = 10\log\left(\frac{1-R}{T}\right) = 10\log\left(\frac{1-|S_{11}|^2}{|S_{21}|^2}\right) \quad (4)$$

SE_T can be deduced from equations (3) and (4) as:

$$SE_T = 20\log(S_{21}) \quad (5)$$

The shielding efficiency values for rGO and SrGO laminates synthesized at various temperatures are compared in Fig. 6a–c. The observations indicated that EMI shielding depends on the frequency. All the produced laminates showed high EMI shielding performance at low frequencies. The EMI shielding effectiveness increased with increasing doping time and

temperature. The 1000SrGO-30 sample with a reaction temperature of 1000 °C and doping time of 30 min revealed the largest EMI SE value of 33.2 dB at 100 MHz, which is 119% larger than that of undoped sample (15.5 dB) with the same sample thickness of 140 μm. The largest EMI SE value of 1000SrGO-30 sample is attributed to its largest conductivity due to the highest n-type doping level with sulfur atom. Fig. 6d presents the EMI shielding contribution from absorption and reflection for 1000 °C samples. In all cases, shielding is dominant by absorption. To elaborate the difference in EMI shielding at particular frequency, Fig. 6e presents the SE_A and SE_R measurements of 1000 °C samples at 100 MHz frequency. EMI shielding improved with doping content, as is visible in all bar charts. Furthermore, shielding efficiency (%) was also determined for 1000 °C samples where 1000SrGO-30 provided >99.9% blockage to the incident radiation at 100 MHz (Fig. 6f).

Several mechanisms for the excellent EMI shielding effectiveness of sulfur-doped graphene laminates are proposed in Fig. 7. The highest contribution for enhanced EMI shielding effectiveness comes from n-doping effect of sulfur atoms, which are responsible for increased electrical conductivity. Sulfur atoms create extra electronic cloud that interacts with incoming radiation and disperses the EM waves through the tightly stacked corrugated graphene layers. Difference in electronegativity of S and C creates local dipoles that lead to polarization effects and enhancement of EMI shielding in S doped graphene laminates. Moreover, oxygen and other residual defects present in the graphene layer also perform as polarization centers that introduce defect polarization relaxation and group electronic dipole relaxation.[32, 33]

Multiple internal reflections also play an important role in scattering of incident radiation. Because the corrugated laminate structure is strongly beneficial to shield the incident radiation, when EM waves strike the shielding material, the directional motion of charge carriers in

graphene laminates form oscillatory currents that consumes a great part of EM wave energy.[34, 35] The electromagnetic waves escaping from the first layer are more likely to meet electronic cloud in preceding layers, which makes it highly probable to shield the incoming radiation. The incident radiation is possible to be reflected and scattered many times before losing the intensity and being dissipated as heat. Such kind of alignment of graphene structures is also suggested to provide enhanced EMI shielding performances in polymer composites.[36, 37]

Theoretically, shielding due to reflection part mainly depends on electrical conductivity of shield and the absorption part depends on various factors, such as dielectric, ohmic, magnetic and heat losses. Graphene based materials is known as an absorption-dominant EMI shielding materials.[11, 35] The absorption dominant shielding behavior can be further increased via addition of S atoms. The improved electrical conductivity due to S doping also influence the polarization effects and ohmic losses. The corrugated structure of laminates further increase the ohmic or heat losses due to availability of more conduction paths, thus attenuating the microwaves and dissipating in the form of heat to increase the overall absorption efficiency of S doped graphene.[3] Although, the reflection part of waves suppress the motion of EM waves travelling through the shield, but it may also lead to damage the component by either reflecting back the waves to shielding device or disturbing the performance of surrounding components. Therefore, the shielding materials with absorption dominant phenomenon are more advantageous to use in broadband applications where components need EMI shielding at the same time when they are emitting EMI radiation such as electronic circuits.[11]

Table 2 provides comparison of recently published results related to EMI shielding of graphene based materials. Thickness is one of the key controlling parameter affecting the EMI shielding results. Large values of EMI shielding can be obtained simply through increasing the

thickness of conductive shield; however, the cost, weight, volume and processing limit the use of thick shields in commercial applications. The S-doped graphene laminates, despite being thinner among the listed EMI shielding materials, provides the best EMI shielding performance. It is of interest that recently, research has been focused towards addition of a second phase (either conducting or magnetic materials, such as Ferrites, magnetic Iron Oxides, ZnO)[12, 38, 39] with graphene to improve EMI shielding, whereas S-doped laminates provide outstanding EMI shielding without the need to add another constituent. Couple with low thickness and avoiding the use of secondary phase, the laminated structure provides an excellent substitute for use as EMI shielding materials and open the door to use heteroatom doping to improve the electrical conductivity and EMI shielding effectiveness of graphene materials. To the best of our knowledge, this is the first report presenting the effects of sulfur doping on EMI shielding of graphene structures that will open a new area of research for controlling the EMI shielding via alteration of the properties of reduced graphene oxide.

Table 2 EMI shielding effectiveness of different graphene based shielding materials

Filler	Matrix	t (mm)	σ (S m^{-1})	SE (dB)	Ref.
rGO	Poly (etherimide)	2.3	0.001	18–22	2013[40]
rGO @ Fe_3O_4	Poly (etherimide)	2.5	–	14–18	2013[41]
rGO	Paraffin wax	2.0	< 0.1	18–29	2014[3]
rGO/δ-Fe_2O_3	PVA	0.36	3	20.3	2014[33]
rGO/MWCNT	Polyaniline	2.5	2950	-98	2013[42]
rGO/ Fe_2O_3	-	1.5	0.001	33.3	2014[43]
rGO/ Fe_3O_4	-	3	700	41	2014[34]
rGO/SnO_2	-	3	1374	45.8	2014[44]
CNF-GN	–	0.22–0.27	800	25–28	2014[45]
rGO/CNT/ Fe_3O_4	-	2	-	37	2015[46]
Fe_3O_4/Graphene Nano sheet	–	0.20–0.25	5000	21–24	2014[10]
rGO/Ba-Ferrite	–	1	98	18	2015[12]
MnO_2 @ Fe-GNS	–	1.5	–	–17.5 (RL)	2015[47]
Graphene Nano sheets	–	0.25	–	17	2015[35]
rGO @ Fe_3O_4	–	2	–	–27.5 (RL)	2013[39]
rGO	–	2	–	–7 (RL)	2011[32]
N-doped graphene	–	5	–	–9(RL)	2014[48]
SrGO Laminates	–	**0.14**	**7500**	**33.2**	**This work**

4 Conclusions

In this article, we reported for the first time that, due to the strong n-type doping contribution of S atom in the doped graphenes, a sulfur-doped reduced graphene oxide (SrGO) laminate provides 47% larger electrical conductivity (75 S cm^{-1}) and 119% larger EMI SE (33.2 dB at 100 MHz) with a very small thickness of 140 μm than the undoped graphene. Considering the simplicity and effectiveness, the chemical S-doping on the graphene oxide is expected to open new field in enhancement of the EMI shielding effectiveness of graphene based materials.

Acknowledgements

This work was supported by the Fundamental R&D Program for Core Technology of Materials and the Industrial Strategic Technology Development Program funded by the Ministry of Trade, Industry and Energy, Republic of Korea and partially by Korea Institute of Science and Technology.

References

1. A. P. Singh, M. Mishra, P. Sambyal, B. K. Gupta, B. P. Singh, A. Chandra and S. K. Dhawan, *Journal of Materials Chemistry A*, 2014, **2**, 3581-3593.
2. L. Kong, X. Yin, X. Yuan, Y. Zhang, X. Liu, L. Cheng and L. Zhang, *Carbon*, 2014, **73**, 185-193.
3. B. Wen, X. X. Wang, W. Q. Cao, H. L. Shi, M. M. Lu, G. Wang, H. B. Jin, W. Z. Wang, J. Yuan and M. S. Cao, *Nanoscale*, 2014, **6**, 5754-5761.
4. S. Kim, J.-S. Oh, M.-G. Kim, W. Jang, M. Wang, Y. Kim, H. W. Seo, Y. C. Kim, J.-H. Lee, Y. Lee and J.-D. Nam, *ACS Applied Materials & Interfaces*, 2014.
5. A. Joshi, A. Bajaj, R. Singh, A. Anand, P. S. Alegaonkar and S. Datar, *Composites Part B: Engineering*, 2015, **69**, 472-477.
6. L. Kheifets, A. A. Afifi and R. Shimkhada, *Environmental Health Perspectives*, 2006, **114**, 1532-1537.
7. M.-S. Cao, X.-X. Wang, W.-Q. Cao and J. Yuan, *Journal of Materials Chemistry C*, 2015, **3**, 6589-6599.
8. S. R. Dhakate, K. M. Subhedar and B. P. Singh, *RSC Advances*, 2015, **5**, 43036-43057.
9. J. Liang, Y. Wang, Y. Huang, Y. Ma, Z. Liu, J. Cai, C. Zhang, H. Gao and Y. Chen, *Carbon*, 2009, **47**, 922-925.
10. W.-L. Song, X.-T. Guan, L.-Z. Fan, W.-Q. Cao, C.-Y. Wang, Q.-L. Zhao and M.-S. Cao, *Journal of Materials Chemistry A*, 2015, **3**, 2097-2107.
11. Z. Chen, C. Xu, C. Ma, W. Ren and H.-M. Cheng, *Advanced Materials*, 2013, **25**, 1296-1300.
12. M. Verma, A. P. Singh, P. Sambyal, B. P. Singh, S. K. Dhawan and V. Choudhary, *Physical Chemistry Chemical Physics*, 2015, **17**, 1610-1618.
13. H. Liu, Y. Liu and D. Zhu, *Journal of Materials Chemistry*, 2011, **21**, 3335-3345.
14. D. Wei, Y. Liu, Y. Wang, H. Zhang, L. Huang and G. Yu, *Nano Letters*, 2009, **9**, 1752-1758.
15. Z. Yang, Z. Yao, G. Li, G. Fang, H. Nie, Z. Liu, X. Zhou, X. a. Chen and S. Huang, *ACS Nano*, 2011, **6**, 205-211.
16. S. Yang, L. Zhi, K. Tang, X. Feng, J. Maier and K. Müllen, *Advanced Functional Materials*, 2012, **22**, 3634-3640.
17. J. Xu, G. Dong, C. Jin, M. Huang and L. Guan, *ChemSusChem*, 2013, **6**, 493-499.
18. Y. G. Zhou, X. T. Zu, F. Gao, H. Y. Xiao and H. F. Lv, *Journal of Applied Physics*, 2009, **105**, -.
19. P. A. Denis, R. Faccio and A. W. Mombru, *ChemPhysChem*, 2009, **10**, 715-722.
20. P. Kumar, U. N. Maiti, K. E. Lee and S. O. Kim, *Carbon*, 2014, **80**, 453-461.
21. P. Kumar, F. Shahzad, S. Yu, S. M. Hong, Y.-H. Kim and C. M. Koo, *Carbon*, 2015, **94**, 494-500.
22. W. Chen, L. Yan and P. R. Bangal, *The Journal of Physical Chemistry C*, 2010, **114**, 19885-19890.
23. H. L. Poh, F. Sanek, A. Ambrosi, G. Zhao, Z. Sofer and M. Pumera, *Nanoscale*, 2012, **4**, 3515-3522.

24. C. Mattevi, G. Eda, S. Agnoli, S. Miller, K. A. Mkhoyan, O. Celik, D. Mastrogiovanni, G. Granozzi, E. Garfunkel and M. Chhowalla, *Advanced Functional Materials*, 2009, **19**, 2577-2583.
25. H. Gao, Z. Liu, L. Song, W. Guo, W. Gao, L. Ci, A. Rao, W. Quan, R. Vajtai and P. M. Ajayan, *Nanotechnology*, 2012, **23**, 275605.
26. J.-e. Park, Y. J. Jang, Y. J. Kim, M.-s. Song, S. Yoon, D. H. Kim and S.-J. Kim, *Physical Chemistry Chemical Physics*, 2014, **16**, 103-109.
27. Z. Wang, P. Li, Y. Chen, J. He, W. Zhang, O. G. Schmidt and Y. Li, *Nanoscale*, 2014, **6**, 7281-7287.
28. Y. Li, J. Wang, X. Li, D. Geng, M. N. Banis, Y. Tang, D. Wang, R. Li, T.-K. Sham and X. Sun, *Journal of Materials Chemistry*, 2012, **22**, 20170-20174.
29. Y. S. Yun, V.-D. Le, H. Kim, S.-J. Chang, S. J. Baek, S. Park, B. H. Kim, Y.-H. Kim, K. Kang and H.-J. Jin, *Journal of Power Sources*, 2014, **262**, 79-85.
30. X. Li, G. Zhu and Z. Xu, *Thin Solid Films*, 2012, **520**, 1959-1964.
31. D. Bi, L. Qiao, X. Hu and S. Liu, *Advanced Materials Research*, 2013, **669**, 144-148.
32. C. Wang, X. Han, P. Xu, X. Zhang, Y. Du, S. Hu, J. Wang and X. Wang, *Applied Physics Letters*, 2011, **98**, -.
33. B. Yuan, C. Bao, X. Qian, L. Song, Q. Tai, K. M. Liew and Y. Hu, *Carbon*, 2014, **75**, 178-189.
34. M. Mishra, A. P. Singh, B. P. Singh, V. N. Singh and S. K. Dhawan, *Journal of Materials Chemistry A*, 2014, **2**, 13159-13168.
35. P. Tripathi, C. R. Prakash Patel, A. Dixit, A. P. Singh, P. Kumar, M. A. Shaz, R. Srivastava, G. Gupta, S. K. Dhawan, B. K. Gupta and O. N. Srivastava, *RSC Advances*, 2015, **5**, 19074-19081.
36. W.-L. Song, M.-S. Cao, M.-M. Lu, J. Yang, H.-F. Ju, Z.-L. Hou, J. Liu, J. Yuan and L.-Z. Fan, *Nanotechnology*, 2013, **24**, 115708.
37. N. Yousefi, X. Sun, X. Lin, X. Shen, J. Jia, B. Zhang, B. Tang, M. Chan and J.-K. Kim, *Advanced Materials*, 2014, **26**, 5480-5487.
38. M. Han, X. Yin, L. Kong, M. Li, W. Duan, L. Zhang and L. Cheng, *Journal of Materials Chemistry A*, 2014, **2**, 16403-16409.
39. C. Hu, Z. Mou, G. Lu, N. Chen, Z. Dong, M. Hu and L. Qu, *Physical Chemistry Chemical Physics*, 2013, **15**, 13038-13043.
40. J. Ling, W. Zhai, W. Feng, B. Shen, J. Zhang and W. g. Zheng, *ACS Applied Materials & Interfaces*, 2013, **5**, 2677-2684.
41. B. Shen, W. Zhai, M. Tao, J. Ling and W. Zheng, *ACS Applied Materials & Interfaces*, 2013, **5**, 11383-11391.
42. T. K. Gupta, B. P. Singh, R. B. Mathur and S. R. Dhakate, *Nanoscale*, 2014, **6**, 842-851.
43. A. Gupta, A. P. Singh, S. Varshney, N. Agrawal, P. Sambyal, Y. Pandey, B. P. Singh, V. N. Singh, B. K. Gupta and S. K. Dhawan, *RSC Advances*, 2014, **4**, 62413-62422.
44. M. Mishra, A. P. Singh, B. P. Singh and S. K. Dhawan, *RSC Advances*, 2014, **4**, 25904-25911.
45. W.-L. Song, J. Wang, L.-Z. Fan, Y. Li, C.-Y. Wang and M.-S. Cao, *ACS Applied Materials & Interfaces*, 2014, **6**, 10516-10523.
46. A. P. Singh, M. Mishra, D. P. Hashim, T. N. Narayanan, M. G. Hahm, P. Kumar, J. Dwivedi, G. Kedawat, A. Gupta, B. P. Singh, A. Chandra, R. Vajtai, S. K. Dhawan, P. M. Ajayan and B. K. Gupta, *Carbon*, 2015, **85**, 79-88.
47. H. Lv, G. Ji, X. Liang, H. Zhang and Y. Du, *Journal of Materials Chemistry C*, 2015, **3**, 5056-5064.
48. W.-D. Xue and R. Zhao, *New Journal of Chemistry*, 2014, **38**, 2993-2998.

Fig. Captions

Scheme. 1 Synthesis of rGO, SrGO-10 and SrGO-30 at three different temperatures..... 19

Fig. 1. (a) TEM image of 1000SrGO-30; (b) SEM image of 1000SrGO-30; (c) GO and 1000SrGO-30; (d-e) EDX analysis and elemental mapping of S from 1000SrGO-30; (f) Cross sectional view of 1000SrGO-30 laminate (inset showing samples for electrical conductivity and EMI shielding)..... 20
Fig. 2 C1s spectra of (a) GO; (b) 1000SrGO-30; S2p spectra of (c) 250SrGO-30; (d) 650SrGO-30; (e) 1000SrGO-30..... 21
Fig. 3 XPS Spectra of (a) 250rGO, 250SrGO-10, 250rGO-30; (b) 650rGO, 650SrGO-10, 650SrGO-30; (c) 1000rGO, 1000SrGO-10, 1000SrGO-30. 22
Fig. 4 Raman spectrum of (a) 1000rGO, 1000SrGO-10, 1000SrGO-30; (b) 650rGO, 650SrGO-10, 650SrGO-30; (c) GO, 250rGO, 250SrGO-10, 250SrGO-30 (Parenthesis show the D to G band intensity ratio); Inset shows the enlarged view of 1000rGO and 1000SrGO-30 spectra with red shift. 23
Fig. 5 Electrical conductivity of doped and undoped graphene laminates 24
Fig. 6 EMI shielding effectiveness of (a) 250rGO, 250SrGO-10 and 250SrGO-30; (b) 650rGO, 650SrGO-10 and 650SrGO-30; (c) 1000rGO, 1000SrGO-10 and 1000SrGO-30; (d) Shielding due to absorption and reflection for 1000rGO, 1000SrGO-10 and 1000SrGO-30; (e) Comparison of shielding due to absorption and reflection for 1000rGO, 1000SrGO-10 and 1000SrGO-30 at 100 MHz; (f) Shielding efficiency for 1000rGO, 1000SrGO-10 and 1000SrGO-30 laminates as function of frequency. 25
Fig. 7 Proposed mechanism for EMI shielding with effect of sulfur doping..... 26

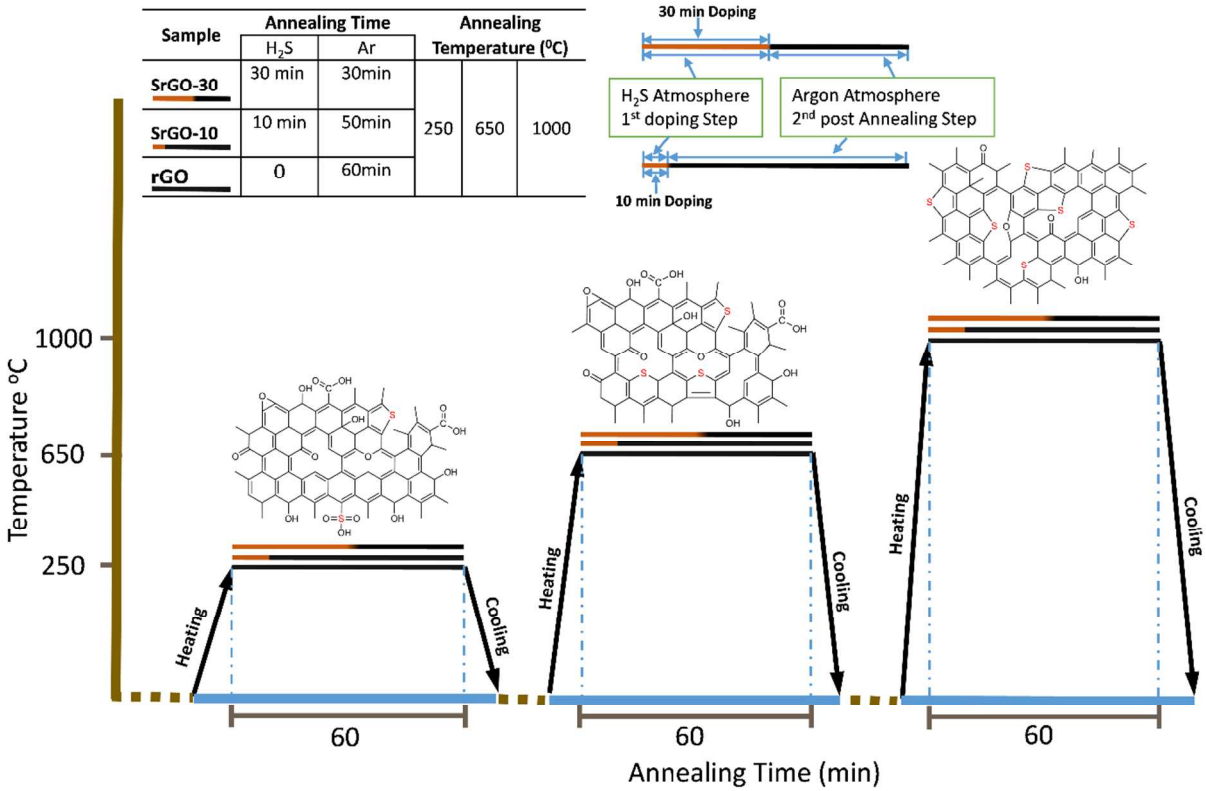

Scheme. 1 Synthesis of rGO, SrGO-10 and SrGO-30 at three different temperatures

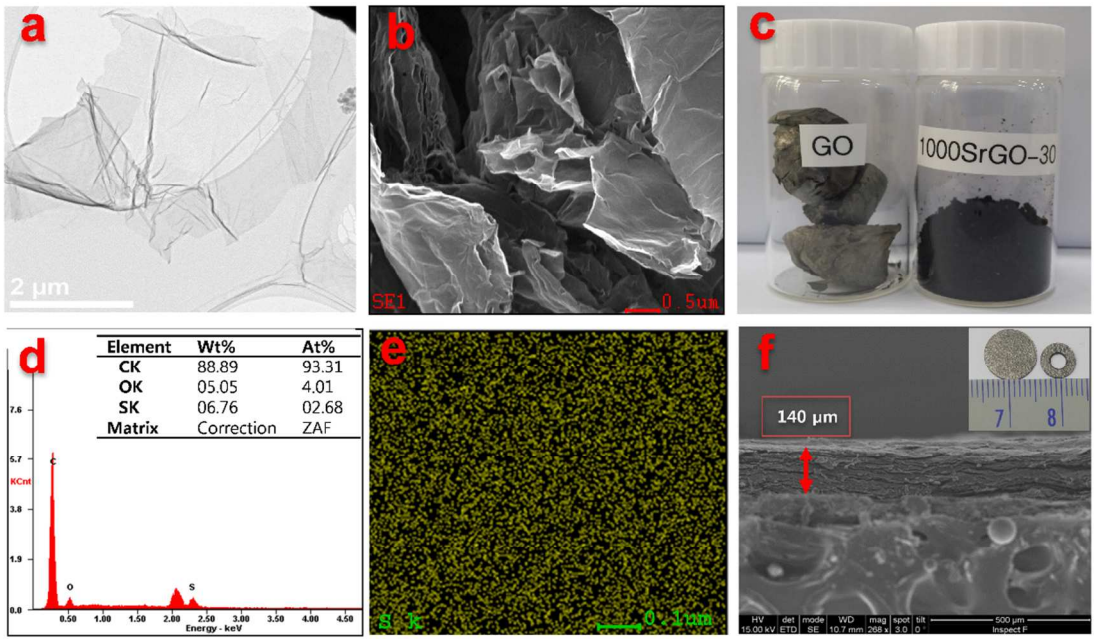

Fig. 1. (a) TEM image of 1000SrGO-30; (b) SEM image of 1000SrGO-30; (c) GO and 1000SrGO-30; (d-e) EDX analysis and elemental mapping of S from 1000SrGO-30; (f) Cross sectional view of 1000SrGO-30 laminate (inset showing samples for electrical conductivity and EMI shielding).

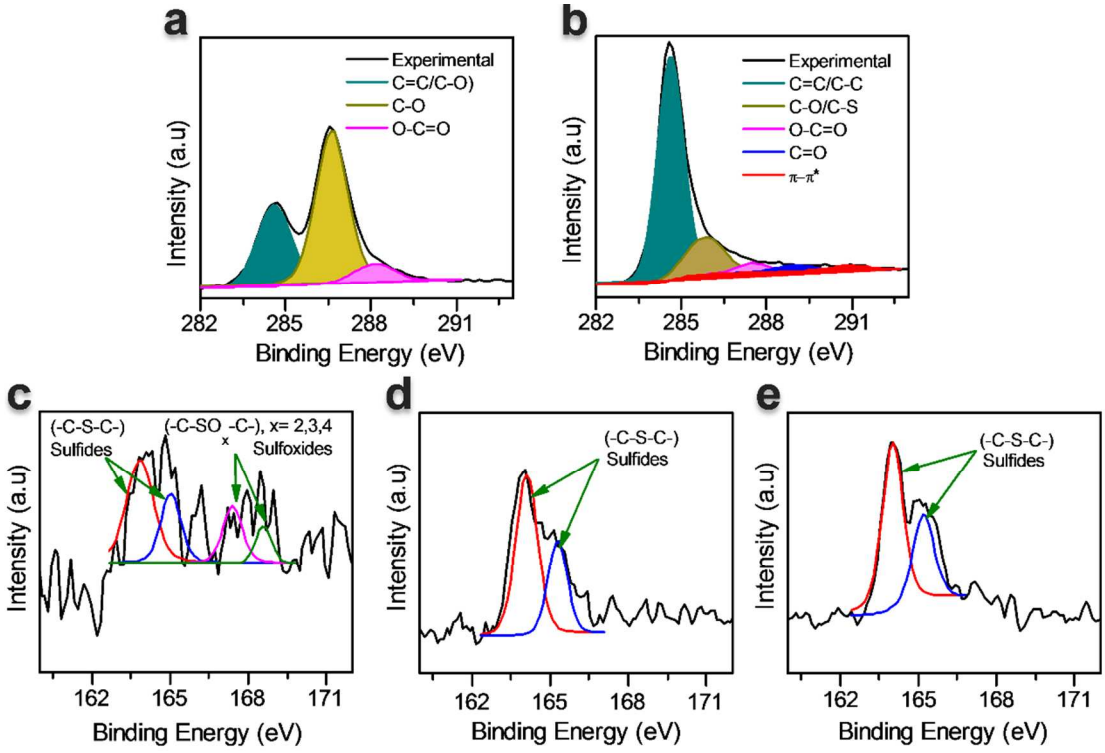

Fig. 2 C1s spectra of (a) GO; (b) 1000SrGO-30; S2p spectra of (c) 250SrGO-30; (d) 650SrGO-30; (e) 1000SrGO-30

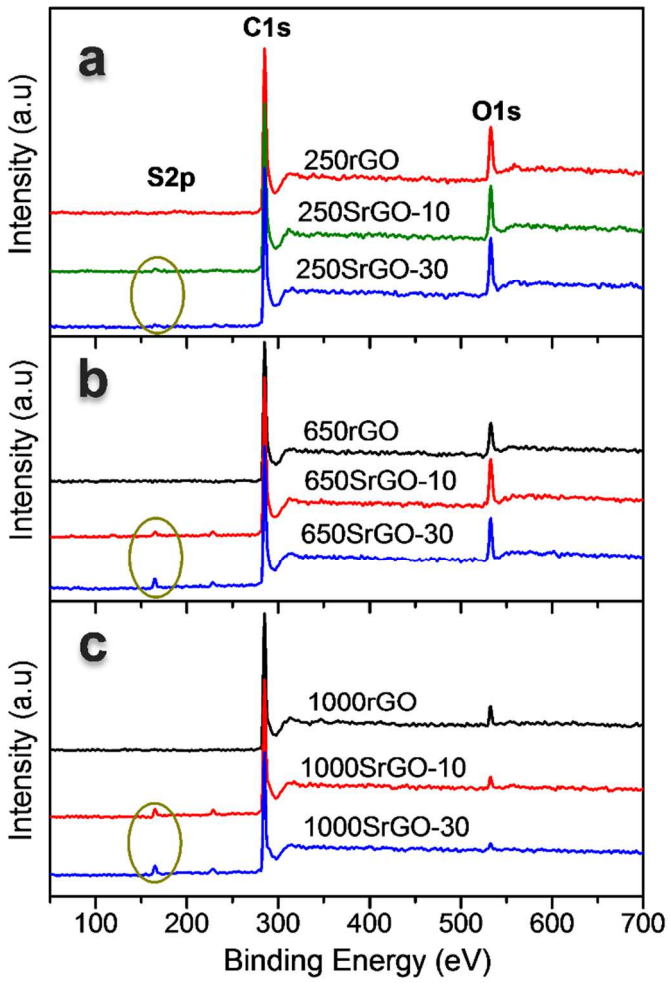

Fig. 3 XPS Spectra of (a) 250rGO, 250SrGO-10, 250rGO-30; (b) 650rGO, 650SrGO-10, 650SrGO-30; (c) 1000rGO, 1000SrGO-10, 1000SrGO-30.

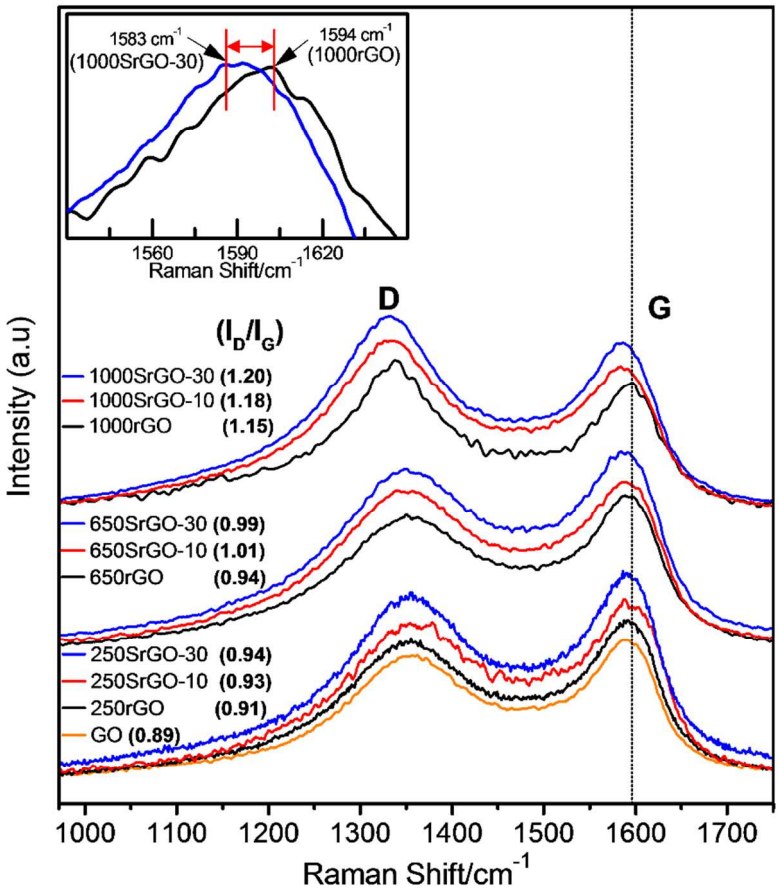

Fig. 4 Raman spectrum of (a) 1000rGO, 1000SrGO-10, 1000SrGO-30; (b) 650rGO, 650SrGO-10, 650SrGO-30; (c) GO, 250rGO, 250SrGO-10, 250SrGO-30 (Parenthesis show the D to G band intensity ratio); Inset shows the enlarged view of 1000rGO and 1000SrGO-30 spectra with red shift.

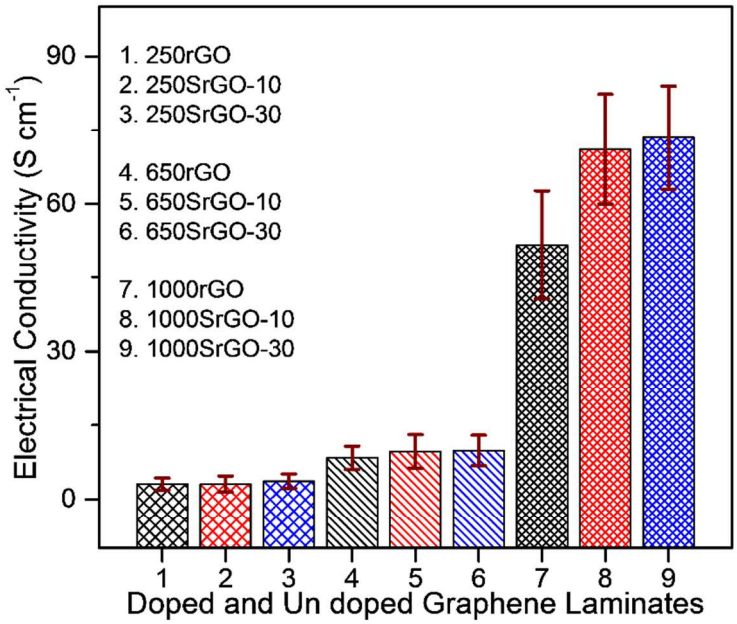

Fig. 5 Electrical conductivity of doped and undoped graphene laminates

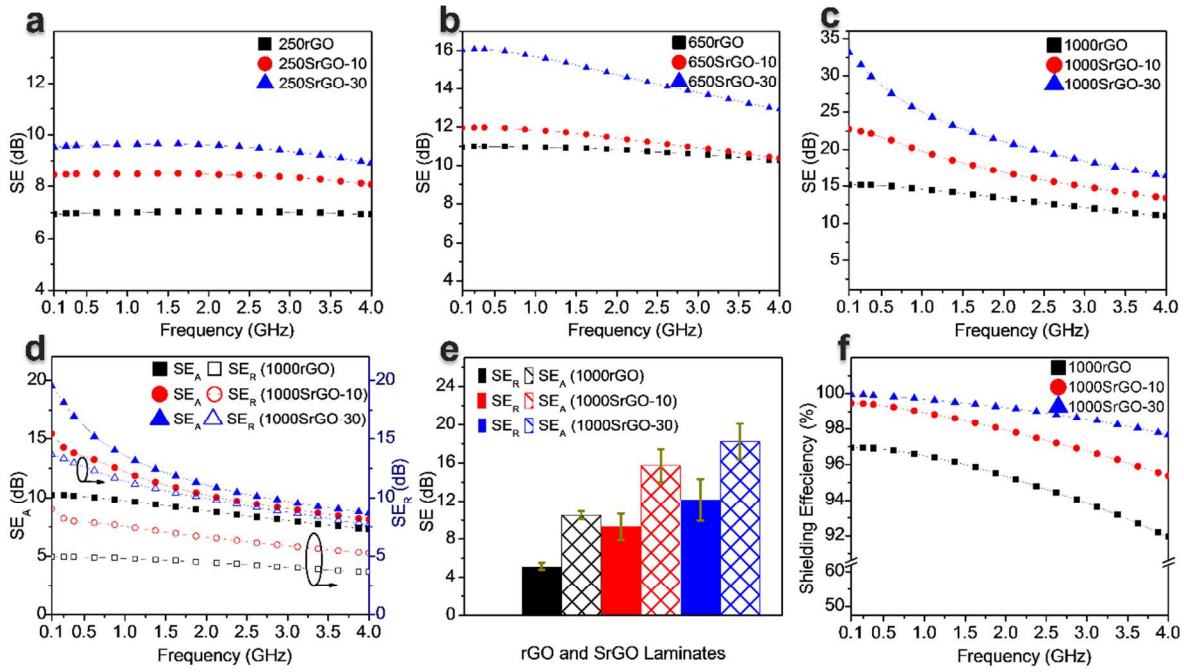

Fig. 6 EMI shielding effectiveness of (a) 250rGO, 250SrGO-10 and 250SrGO-30; (b) 650rGO, 650SrGO-10 and 650SrGO-30; (c) 1000rGO, 1000SrGO-10 and 1000SrGO-30; (d) Shielding due to absorption and reflection for 1000rGO, 1000SrGO-10 and 1000SrGO-30; (e) Comparison of shielding due to absorption and reflection for 1000rGO, 1000SrGO-10 and 1000SrGO-30 at 100 MHz; (f) Shielding efficiency for 1000rGO, 1000SrGO-10 and 1000SrGO-30 laminates as function of frequency.

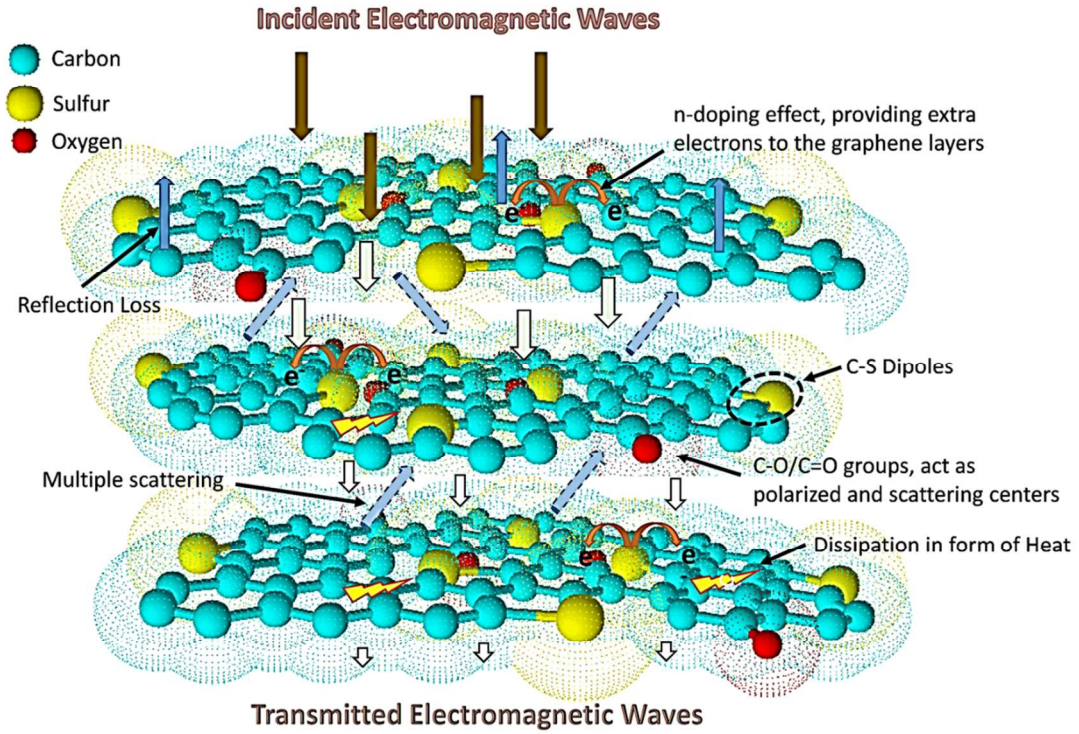

Fig. 7 Proposed mechanism for EMI shielding with effect of sulfur doping

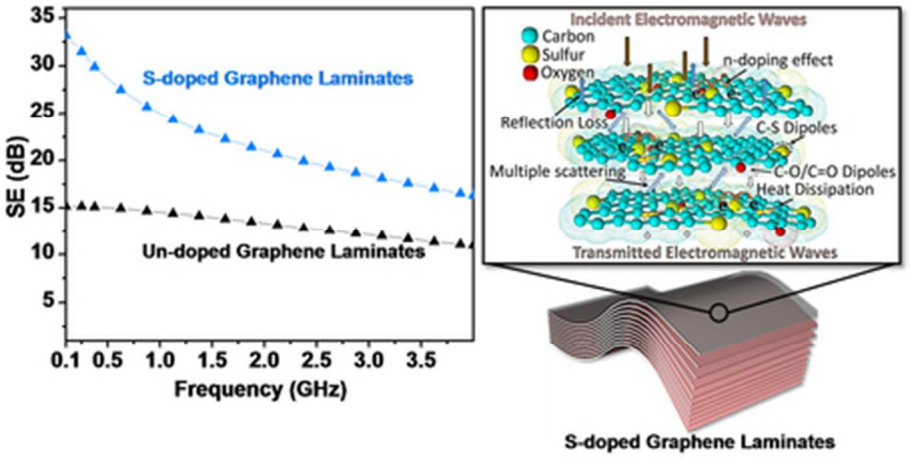

38x19mm (300 x 300 DPI)